10.1109/PVSC.2013.6744324

# Analytical drift-diffusion modeling of GaAs solar cells incorporating a back mirror

Matthew P. Lumb[1,2], Christopher G. Bailey[1] Jessica G. J. Adams[3], Glen Hillier[3], Francis Tuminello[3], Victor C. Elarde[3] and Robert J. Walters[1]

[1] US Naval Research Laboratory, Washington DC, 20375, USA
[2] The George Washington University, 2121 I Street NW, Washington DC, 20037, USA
[3] MicroLink Devices, 6457 Howard Street, Niles, IL 60714, USA

***Abstract*** **In this work we extend the analytical drift-diffusion model, or Hovel model, to model the electrical characteristics of solar cells incorporating a back mirror. We use a compact summation approach to derive modified optical generation functions in homojunction solar cells, considering both coherent and incoherent reflections from the back reflector. We use the model to simulate the performance of a real GaAs solar cell device fabricated using an epitaxial-lift-off procedure, demonstrating excellent agreement between the simulated and measured characteristics. We also calculate the performance of the same solar cell with different back reflectors, including metal mirrors and a distributed Bragg reflector.**

***Index Terms*** **— Semiconductor device modeling, Photovoltaic cells, Reflection.**

## I. Introduction

The drift-diffusion problem is a well-established model for predicting the performance of optoelectronic devices, including solar cells. The problem can be solved analytically, and while numerical solvers generally allow greater flexibility in the specific device structures that can be modeled, solar cells can be modeled analytically in a very efficient way. For the analytical solution to be accurate, the solar cells must satisfy the requirements for the specific boundary conditions applied to the charge-transport equations, which allow the mathematical separation of the field-bearing and quasi-neutral regions (QNR) of the solar cell.

This analytical approach used to model solar cells was developed in the 1970s and is often called the Hovel, or Hovel-Woodall model, after the names of the researchers who made the early developments of the model in a series of landmark publications [1, 2]. Although widely accepted, an obvious drawback is in the simplicity of the generation function used. The photon flux in the solar cell medium is assumed to follow a Beer-Lambert type function, which is a good assumption for materials with no highly reflecting interfaces. However, the use of reflecting surfaces to boost the photocurrent production of current state of the art solar cells is now a commonplace technology. Although work has been done to calculate the generation functions of thin-film solar cells with a variety of back reflection properties, until recently, no derivation of the analytical expressions for the photocurrent had been published and models are restricted to numerical approaches [3-7]. An analytical drift-diffusion model developed at the Naval Research Laboratory, coupled with a detailed III-V optical properties and material parameters database, has been used to simulate the characteristics of single [8] and multi-junction [9] III-V solar cells lattice matched to InP. This model was the basis of an extension to the Hovel model to incorporate the effects of a planar back mirror [10].

The challenge in simulating mirrored solar cells using an analytical drift diffusion model arises from the complicated generation function when multiple reflections in the structure occur. Calculating the photon flux in a one-dimensional multilayer is straightforward using a transfer matrix method [11], but the expanded expressions describing the position dependent flux become prohibitively complicated for relatively few layers. In our recent publication [10], we used a compact summation method based on the simple case of a homojunction with non-zero front and rear reflectivity to produce a full solution to the analytical model, examining both coherent and incoherent reflections [12]. This derivation is going to form the basis of the work we present here. The full derivation is not included in this paper, and readers are directed to reference [10] for a full mathematical derivation. However, in this work we will use the model to simulate GaAs solar cells employing different back reflectors, and discuss the relative merits of using different metals and a multilayered distributed Bragg reflector (DBR).

## II. Back Reflection

In this section we describe the generation functions adopted for the three cases considered in this model, no back-reflection, incoherent back reflection and coherent back reflection. In order to achieve coherent back reflection, the thickness of the solar cell must be thin enough such that the forward and reverse propagating fields maintain coherence over the whole structure. In very thick materials, such as substrates with thicknesses of the order of hundreds of microns, scattering from impurities, defects and material inhomogeneities lead to a loss of coherence. However, typical III-V single junction thicknesses are under 10 microns, and are thin enough to support coherent reflection. In addition, the front surface and back-mirror interface must be planar to maintain coherent reflections.

In this work we adopt a similar nomenclature for the thicknesses of the layers in the solar cell as Fonash [13], and Fig. 1 shows the layer structure for the cell and the naming scheme. The emitter and base thicknesses are denoted $X_e$ and $X_b$ respectively and the depletion widths in each layer are we and $w_b$ for the emitter and base respectively. The thickness of the quasi-neutral region in the emitter is $d_1 = X_e - w_e$ and the thickness of the QNR in the base is $d_2 = X_b - w_b$. The total depletion width of the structure is given by $W = w_e + w_b$. The reflectivity of the front and rear surfaces of the solar cell are denoted $R_1$ and $R_2$ respectively and the total thickness of the solar cell is the sum of the n-type QNR, the depletion region and the p-type QNR, $P = d_1 + W + d_2$. The emitter and base of the solar cell are assumed to be the same material and, for simplicity, the cell is assumed to not contain a window or back surface field layer.

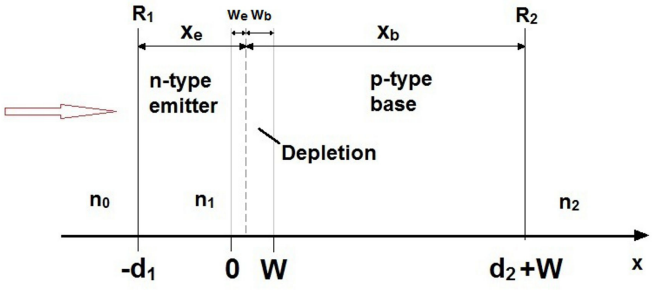


Fig. 1. A schematic diagram of the layer structure and naming scheme for the analytical solar cell model.

Within the n-type QNR for the example in Fig. 1, the minority hole density, $p$, as a function of position satisfies

$$\frac{d^2p}{dx^2} - \frac{p - p_0}{L_p^2} + \int \frac{\alpha\varphi(x)}{D_p} dE = 0 \qquad (1)$$

where $p_0$ represents the minority carrier (hole) density under equilibrium conditions and $L_p$ and $D_p$ represent the minority carrier diffusion length and diffusivity, respectively. The absorption coefficient of the material is given by $\alpha$ and $\varphi(x)$ describes the photon flux as a function of depth in the cell. For the case of no back reflection, $\varphi(x)$ is described by the Beer-Lambert law as follows:

$$\varphi(x) = (1 - R_1)\varphi_0 e^{-\alpha(x+d_1)} \qquad (2)$$

Here $R_1$ is the reflectance of the front surface of the solar cell and $\varphi_0$ is the flux incident on the solar cell. The expression for the current can be derived by solving equation 1 and applying the boundary conditions arising from the requirement of current continuity. A detailed derivation can be found in Fonash, and the full result is presented in reference [10].

In the case of incoherent back reflection, the intensities of the multiple reflected beams add at all positions in the cell. The flux at position $x$ can be found from the sum of all the reflected beams and can be expressed as a geometric progression

$$\varphi(x) = (1 - R_1)\frac{\varphi_0\left(e^{-\alpha(x+d_1)} + e^{-2\alpha P}R_2 e^{\alpha(x+d_1)}\right)}{1 - R_1R_2e^{-2\alpha P}} \qquad (3)$$

By solving equation 1 with this equation describing the photon flux, it is possible to derive a new formalism for the current density in each of the regions of the solar cell.

In the case of coherent back reflection, the phase of the multiple reflected beams is conserved and thus the forward and reverse propagating fields interfere. For an electric field impinging on the top surface of the solar cell with amplitude $E_0$, the field amplitude after successive reflections in the solar cell is shown schematically in Fig. 2. The same geometric progression technique can be applied to derive the field intensity at all points in the structure, and the result is given in equation 4, describing the flux at position x in the case of coherent back reflection. As before, this expression can be substituted into equation 1 and solved to give the current density with coherent back reflection.

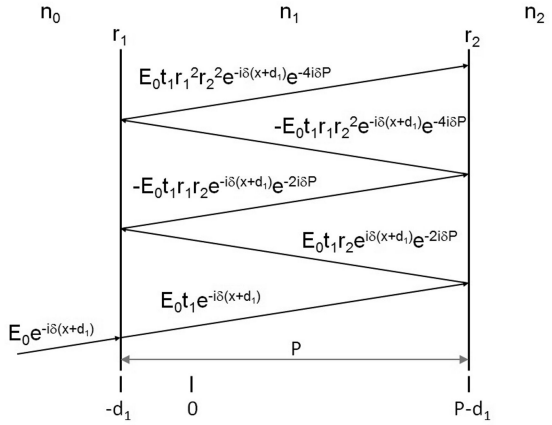


Fig. 2. A simplified view of the multiple coherent reflections in the solar cell. For illustrative purposes the reflections are shown at oblique incidence but the field amplitudes are derived for normal incidence.

$$\begin{aligned}\varphi(x) = (1 - R_1) \times \Big\{ & \varphi_0 \Big( e^{-\alpha(x+d_1)} \\ & + e^{\alpha(x+d_1)} e^{-2\alpha P} R_2 \\ & + e^{-\alpha P} \left[ r_2 e^{i\frac{4\pi}{\lambda} n(x+d_1-P)} \right. \\ & \left. + r_2^* e^{-i\frac{4\pi}{\lambda} n(x+d_1-P)} \right] \Big) \Big\} \\ & / \left\{ e^{-\alpha P} \left[ r_1 r_2 e^{-i\frac{4\pi}{\lambda} nP} + r_1^* r_2^* e^{i\frac{4\pi}{\lambda} nP} \right] \right. \\ & \left. + e^{-2\alpha P} R_1 R_2 + 1 \right\}\end{aligned} \qquad (4)$$

## III. Comparison To Experimental Data

To investigate the effectiveness of the model for simulating real solar cell devices, a high efficiency GaAs single junction solar cell was grown by MOCVD and fabricated at MicroLink Devices, Inc. The device uses MicroLink's proprietary epitaxial lift-off technology to remove the substrate and incorporate a thick Ag mirror on the back surface with a 5Å proprietary adhesion layer. The device design is summarized in Table 1.

Table 1.
The solar cell structure grown and fabricated at MicroLink Devices.

| Layer | Material | Thickness (Å) | Doping ($cm^{-3}$) | SRV (cm/s) |
|---|---|---|---|---|
| Window | $Al_{0.53}In_{0.47}P$ | 165 | n $1\times10^{18}$ | $5\times10^{6}$ |
| Emitter | GaAs | 500 | n $2\times10^{18}$ | $6.5\times10^{4}$ |
| Base | GaAs | 9100 | p $5\times10^{17}$ | $5.0\times10^{4}$ |
| BSF | $In_{0.49}Ga_{0.51}P$ | 300 | p $1\times10^{18}$ | n/a |
| Transparent back contact | $Al_{0.3}Ga_{0.7}As$ | 3000 | p $>4\times10^{18}$ | n/a |
| Adhesion layer | n/a | 5 | n/a | n/a |
| Mirror | Ag | Thick | n/a | n/a |

The full solar cell structure has a significantly more complicated layer structure than the simple np diode shown schematically in Fig. 1. The structure incorporates a window layer, back-surface field layer and a transparent back contact layer. To account for this added complexity, the reflectivity of the front surface in an air ambient, $r_1$ in Fig. 2, is now the reflectivity of the GaAs and AlInP window combined, calculated using the standard transfer matrix technique. The AlInP optical constants were taken from a recent publication by Homier *et al*. [14] The rear surface reflectivity, $r_2$, is the combined reflectivity of the Ag mirror, adhesion layer, AlGaAs contact layer and BSF layer, in a GaAs ambient. These values of $r_1$ and $r_2$ were then used in the equations derived for coherent reflection and used to generate the EQE and IV characteristics of the solar cell.

To account for the contribution of the window layer to the EQE, a standard approach described elsewhere was used [15, 16]. This is a good approximation as the window absorbs at short wavelengths, well away from the part of the spectrum where multiple reflections from the back-reflector occur. To account for the absorption in the window, the same argument was used and thus the flux transmitted through the window was attenuated using the Beer-Lambert law. To make the fringes in the EQE clearly visible, no anti-reflection coating was applied to the structure. The surface recombination velocities in the emitter, window and base, were chosen to give the best fit of the calculated EQE curve to the measured data. The SRH lifetimes of both electrons and holes were chosen to be 20ns.

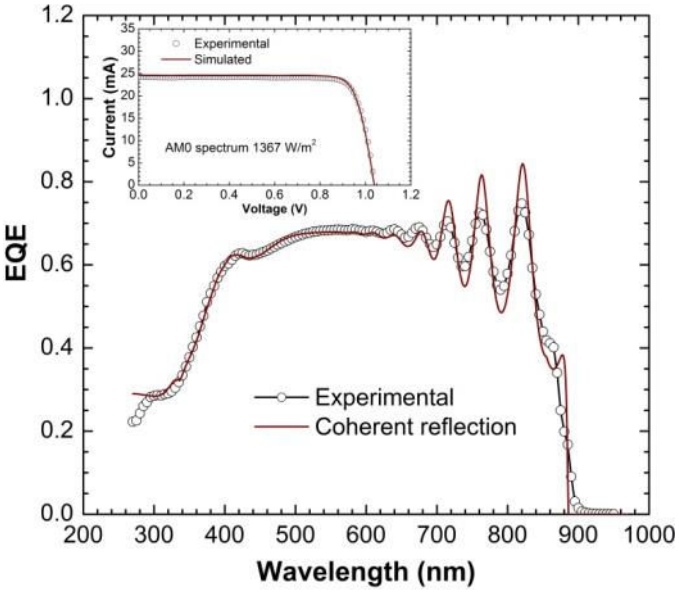


Fig. 3. The measured EQE for the GaAs ELO solar cell with an Ag back mirror (circles) and the modeled EQE including coherent reflection (solid line) (Inset) The measured LIV under the AM0 spectrum, alongside the modeled LIV with coherent back-reflection.

Fig. 3 shows the modeled EQE with and without the coherent back reflector, alongside the measured EQE of the device. The coherent reflection model clearly reproduces the experimental data very accurately. However, the fringes in the EQE are slightly more pronounced in the model than in the data, primarily due to the resolution limit of the spectrometer, but this may also indicate a small amount of incoherent reflection. The inset to Fig. 3 shows the measured LIV curve of the device under 1-sun AM0 illumination, along with the modeled curve. In the simulation, a series resistance of 2.1 $\Omega cm^2$ was applied to improve the fit to the experimental data. The total device area was 1.108 $cm^2$ and the exposed area of the device was 0.998 $cm^2$. The measured and modeled figures of merit for the solar cell are summarized in Table 2, demonstrating good agreement with theory and experiment. The main sources of uncertainty in these figures of merit arise from the uncertainty in the absolute measurement of EQE and the accuracy of the simulated AM0 spectrum.

Table 2.
A comparison of the measured and modeled figures of merit of the single junction solar cell.

| Parameter | Measured | Model |
|---|---|---|
| Isc (mA) | 24.3 | 24.5 |
| $V_{oc}$ (V) | 1.041 | 1.039 |
| $P_{max}$ (mW) | 20.9 | 21.3 |
| FF (%) | 82.9 | 83.7 |

## IV. Different Back Reflectors

The impact of using different back surface reflectors (BSRs) on the EQE of the GaAs solar cell was established by

simulating the GaAs solar cell with three BSR types. The standard BSR was the Ag mirror, as described in Table 1. In addition, an Au back reflector was simulated, using the same layer structure described in Table 1. Finally, the metal mirrors were replaced with a DBR. DBRs consist of alternate high and low index layers, each with a quarter-wave optical thickness, where the wavelength is the Bragg condition, corresponding to the center of the high-reflectivity stopband. The DBR simulated here consisted of 20 periods of $Al_{0.1}Ga_{0.9}As/Al_{0.95}Ga_{0.05}As$ high and low index layers respectively. The Bragg wavelength of the structure was set at 840 nm, which is slightly shorter wavelength than the GaAs bandgap. This allows the long wavelength side of the DBR stopband to be roughly coincident with the absorption edge of the GaAs absorber layers, and also allows the high reflectivity stopband to penetrate into the spectral response region of the GaAs solar cell. The DBR structure is summarized in Table 3.

TABLE 3.
THE 20 PERIOD DBR STRUCTURE INCORPORATED INTO THE SINGLE JUNCTION SOLAR CELL MODEL.

| Layer | Material | Thickness (Å) | Periods |
|---|---|---|---|
| $n_H$ | $Al_{0.1}Ga_{0.9}As$ | 588 | x20 |
| $n_L$ | $Al_{0.95}Ga_{0.05}As$ | 727 | |

The reflectivity of each mirror in a GaAs ambient is shown in Fig. 4(a). For the metal mirrors, the reflectivity is simply the reflectivity at the GaAs/metal interface, whereas the DBR structure is the reflectivity at the GaAs/DBR interface and assumes a semi-infinite GaAs substrate beneath the DBR. The Ag mirror has higher reflectivity than the Au mirror over the whole spectral range, in particular at short wavelengths. The DBR has reflectivity close to unity across the stopband region, but has much lower reflectivity than both metal mirrors outside this region. The stopband width of the DBR was approximately 110 nm, which can be improved by choosing materials with a greater index contrast. However, the composition of the high index $Al_xGa_{1-x}As$ layer was limited to approximately x=0.1, as the reflectivity of the DBR is penalized if either of the layers in one period are absorbing in the range of the stopband.

The actual reflectivity at the rear surface of the solar cell, corresponding to $R_2$ in Fig 1. is slightly different to the GaAs/mirror reflectivity due to the presence of the BSF layer, buffer layer and, in the case of the metal mirrors, the adhesion layer. The total reflectivity of the BSF/Buffer/mirror structure in a GaAs ambient is shown in Fig. 4(b). The absorption of the BSF and buffer layers cuts the reflectivity at short wavelengths and therefore the Ag and Au mirrors have near identical performance below approximately 700 nm. At longer wavelengths the Ag mirror has slightly higher reflectivity than the Au mirror. The reflectivity of the back surface with the DBR is largely unaffected by the presence of the buffer and BSF layers.

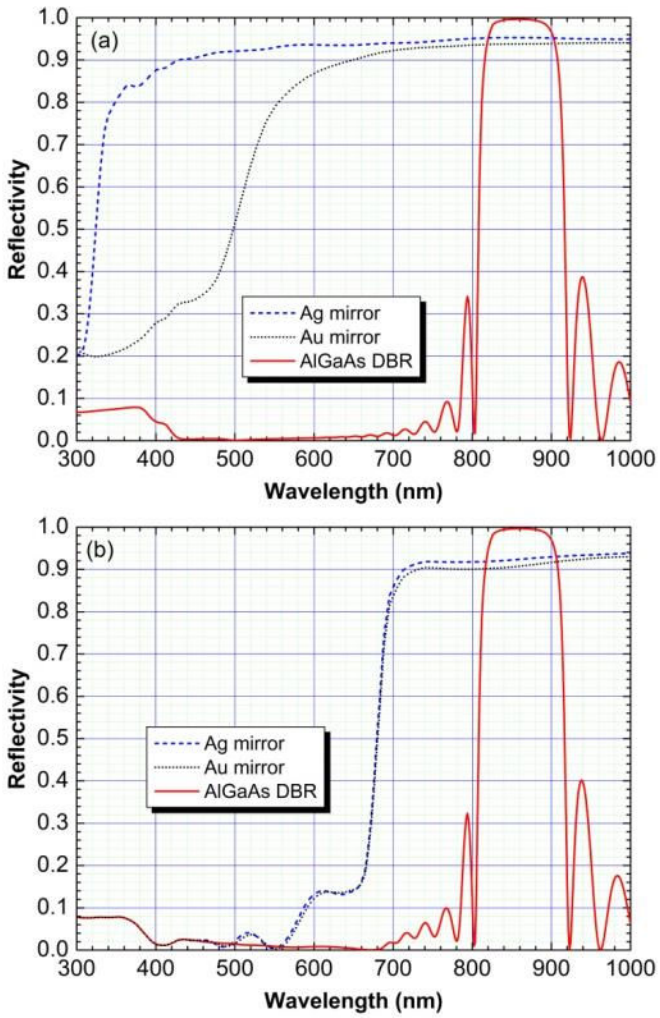


Fig. 4. (a) The calculated reflectivity at an interface between GaAs and an Ag mirror, Au mirror and a 20 period AlGaAs DBR (b) The calculated total back surface reflectivity of the solar cell including the BSF, buffer layer and adhesion layer with an Ag mirror, Au mirror and DBR.

In Fig. 5, the calculated EQE for the GaAs device described in Table 1 is shown for the three different BSRs in Fig. 4(b). The EQE of the Ag and Au mirrors are extremely similar, with AM0 short circuit current densities within 0.12% of one another. However, the DBR EQE curve is significantly different to the metal mirrors. The EQE close to the bandedge of the GaAs is strongly enhanced due to the reflectivity of the DBR approaching unity, which is particularly important in the region where the GaAs is weakly absorbing. However, the response at wavelength shorter than 800 nm is lower than the metal mirrors due to the finite stop-band width of the DBR. As a result, the short circuit current density is approximately 1.6% lower than with the Ag mirror. However, the high reflectivity of the DBR at the bandedge of the GaAs will be particularly useful for recycling of the photons emitted through radiative recombination, an effect which is currently not included in this model. Extension of the model to incorporate this effect will be the subject of further study.

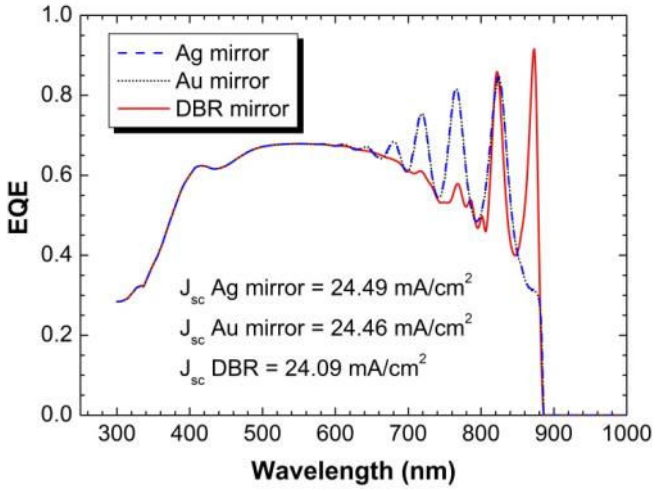


Fig. 5. The EQE of the GaAs solar cell with an Ag mirror, Au mirror and 20 period DBR.

## V. Conclusion

In this paper we have presented calculations of the performance of a single junction GaAs cell using a one-dimensional Hovel model extended to include the effect of both coherent and incoherent back reflection. A summation approach was used to derive compact analytical generation functions for the two cases. We have compared the model prediction to data from a real GaAs device fabricated using an ELO technique, incorporating an Ag back reflector. The model was able to accurately reproduce the shape of the EQE curve and accurately predict the figures of merit derived from the LIV curve of the device under 1-sun AM0 illumination. The same solar cell was also modeled using an Au back reflector, and a 20 period AlGaAs based DBR. The performance of the metal mirrors is very similar due to their similar reflectivity. The DBR produces a strong enhancement of the EQE in the region of the high-reflectivity stopband, but overall provides lower enhancement to the photocurrent than the metal mirrors due to the limited width of the stopband.

## Acknowledgements

The authors are extremely grateful to Dr. I. Vurgaftman and Dr. M. González for many helpful discussions and suggestions during in the preparation of this paper. This work was supported by the Office of Naval Research

## References

[1] H. J. Hovel and J. M. Woodall, "The effect of depletion region recombination currents on the efficiencies of Si and GaAs solar cells," in *10th IEEE Photovoltaics Specialist Conference*, Palo Alto, California, 1973, p. 25.

[2] H. J. Hovel, *Solar Cells* vol. II. New York: Academic Press, 1975.

[3] P. A. Basore, "Numerical modeling of textured silicon solar cells using PC-1D," *IEEE Trans. Electron Devices,* vol. 37, pp. 337-343, Feb 1990.

[4] G. Létay, M. Hermle, and A. W. Bett, "Simulating single-junction GaAs solar cells including photon recycling," *Prog. Photovolt: Res. Appl.,* vol. 14, pp. 683-696, May 2006.

[5] Z. Q. Li, Y. G. Xiao, and Z. M. S. Li, "Two-dimensional simulation of GaInP/GaAs/Ge triple junction solar cell," *Phys. Status Solidi C,* vol. 4, pp. 1637-1640, Apr 2007.

[6] R. Stangl, M. Kriegel, and M. Schmidt, "AFORS-HET, version 2.2, a numerical computer program for simulation of heterojunction solar cells and measurements," in *Conference Record of the 2006 IEEE 4th World Conference on Photovoltaic Energy Conversion*, Waikoloa, Hawaii, 2006, pp. 1350-1353.

[7] J.-Y. Chang, S.-H. Yen, Y.-A. Chang, and Y.-K. Kuo, "Simulation of High-Efficiency GaN/InGaN p-i-n Solar Cell With Suppressed Polarization and Barrier Effects," *IEEE J. Quantum Electron.,* vol. 49, pp. 17-23, Jan 2013.

[8] M. P. Lumb, M. González, I. Vurgaftman, J. R. Meyer, J. Abell, M. K. Yakes, R. Hoheisel, J. G. Tischler, P. P. Jenkins, P. Stavrinou, M. Fuhrer, N. J. Ekins-Daukes, and R. J. Walters, "Simulation of novel InAlAsSb solar cells," in *Proceedings of SPIE, Physics and Simulation of Optoelectronic Devices*, San Francisco, 2012, p. 82560S.

[9] M. P. Lumb, M. González, C. G. Bailey, I. Vurgaftman, J. R. Meyer, J. Abell, M. Yakes, R. Hoheisel, J. G. Tischler, P. N. Stavrinou, M. Fuhrer, N. J. Ekins-Daukes, and R. J. Walters, "Drift-diffusion modeling of InP-based triple junction solar cells," in *Proceedings of SPIE, Physics and Simulation of Optoelectronic Devices*, San Francisco, 2013, p. 86201G.

[10] M. P. Lumb, C. G. Bailey, J. G. J. Adams, G. Hillier, F. Tuminello, V. C. Elarde, and R. J. Walters, "Extending the One-Dimensional Hovel Model for Coherent and Incoherent Back Reflections in Homojunction Solar Cells," *IEEE J. Quantum Electron.,* vol. 49, pp. 462-470, 2013.

[11] O. S. Heavens, *Optical Properties of Thin Solid Films*. London: Butterworths, 1955.

[12] B. Harbecke, "Coherent and incoherent reflection and transmission of multilayer structures," *Appl. Phys. B,* vol. 39, pp. 165-170, Nov 1986.

[13] S. J. Fonash, *Solar Cell Device Physics*, 2nd ed. New York: Academic Press, 2010.

[14] R. Homier, A. Jaouad, A. Turala, C. E. Valdivia, D. Masson, S. G. Wallace, S. Fafard, R. Ares, and V. Aimez, "Antireflection Coating Design for Triple-Junction III-V/Ge High-Efficiency Solar Cells Using Low Absorption PECVD Silicon Nitride," *IEEE J. Photovolt.,* vol. 2, pp. 393-397, Jul 2012.

[15] X. M. Dai and Y. H. Tang, "A simple general analytical solution for the quantum efficiency of front-surface-field solar cells," *Sol. Energy Mater. Sol. Cells,* vol. 43, pp. 363-376, Oct 1996.

[16] A. Belghachi and A. Helmaoui, "Effect of the front surface field on GaAs solar cell photocurrent," *Sol. Energy Mater. Sol. Cells,* vol. 92, pp. 667-672, Feb 2008.